Chapter 9
Contemporary Discoveries in the Copper Octacyanidometallate Photomagnetic Assemblies

Olaf Stefanczyk, Koji Nakabayashi, and Shin-ichi Ohkoshi

Abstract In this chapter, the concept of photomagnetic effect in copper(II)-octacyanidometallate(IV) systems and its various aspects have been introduced. Multifunctional cyanido-bridged metal assemblies attract much attention due to their great importance for fundamental research as well as their potential application in various technologies. Among the numerous advantages of this type of assemblies, the vast structural diversity should be distinguished, as it allows for various electronic states by a combination of metal ions and ligand, resulted in their functionalities. The most excellent examples of such materials are photomagnetic compounds revealing switching between different magnetic states by stimulation with electromagnetic radiation. Herein, various Cu^{II}-$[M^{IV}(CN)_8]^{4-}$ complexes with unique characters of photoinduced magnetization, milestones in understanding the mechanism of photomagnetic behavior and the impact of various factors on their photomagnetic phenomena are presented.

9.1 Introduction

Modern chemistry focuses on the elaboration of innovative functional materials and the discovery of new physical phenomena, which can broaden our knowledge and possibly beget new areas of science [1, 2]. Among the available pool of known chemical compounds, multifunctional molecular materials which consist of metal complexes have attracted significant attention by offering several incredible advantages such as the possibility of introducing desirable function at the design stage,

O. Stefanczyk · K. Nakabayashi · S. Ohkoshi (✉)
Department of Chemistry, School of Science, The University of Tokyo, 7-3-1 Hongo, Bunkyo-ku, Tokyo 113-0033, Japan
e-mail: ohkoshi@chem.s.u-tokyo.ac.jp

O. Stefanczyk
e-mail: olaf@chem.s.u-tokyo.ac.jp

K. Nakabayashi
e-mail: knakabayashi@chem.s.u-tokyo.ac.jp

K. Yamanouchi et al. (eds.), *Progress in Photon Science*, Springer Series in Chemical Physics 125, https://doi.org/10.1007/978-3-030-77646-6_9

easiness of synthesis and modification, structural diversity with various topologies [3], the prospect of postsynthetic modification, ability to respond to chemical and physical external stimuli [4, 5], and the most motivating possibility of observing physical cross-effects. All these benefits we owe to the modular construction of these materials based on different combinations of metal cations and ligands which provide various structures and intrinsic functionalities.

Since the beginning of the millennium, multifunctional molecule-based magnetic materials have celebrated a series of great successes in broadening our knowledge about new physical phenomena including novel cross-effects [3, 6, 7]. Scientists were able to combine magnetic phenomena of long-range magnetic ordering (extended two- (2D) and three-dimensional (3D) coordination polymers), slow magnetic relaxation (discrete complexes and clusters, and low-dimensional coordination polymers), or spin transition (monometallic spin crossover and bimetallic charge transfer systems) with other functionalities (e.g. luminescence, nonlinear optical activity, ferroelectricity, conductivity, porosity/sorption). This unique approach resulted in the invention of remarkable materials revealing new magneto-optical cross-effects [8] of magnetic circular dichroism (MCD) in cyanido-bridged Mn^{II}-$[Cr^{III}(CN)_6]^{3-}$ and Mn^{II}-$[Nb^{IV}(CN)_8]^{4-}$ ferrimagnets [9, 10], magneto-chiral dichroism (MChD) in an oxalate-bridged Mn^{II}-Cr^{III} ferromagnet [11], and magnetization-induced second harmonic generation (MSHG) in a cyanido-bridged Co^{II}-$[Cr^{III}(CN)_6]^{3-}$ [12], Mn^{II}-$[Nb^{IV}(CN)_8]^{4-}$ [13, 14] and Mn^{II}-$[Mo^{I}(CN)(NO)]^{3-}$ ferrimagnets [15], and an oxalate-bridged Mn^{II}-Cr^{III} ferromagnet [16]. All compounds exhibit enhancement of nonlinear optical signals by the onset of long-range magnetic ordering below the critical temperature. Besides, nonlinear optical active chiral magnets are worth to emphasize other luminescent magnets combining nontrivial magnetic characteristics with luminescence phenomena [17–20]. Other noteworthy classes of assemblies are systems revealing simultaneously ferroelectricity and ferromagnetism [21, 22], and superionic conductivity and ferromagnetism—V^{II}/Co^{II}-$[Cr^{III}(CN)_6]_{2/3}\cdot zH_2O$ [23]. Last but not least, there is also successively explored family of compounds showing diverse magnetic response towards sorption and desorption of solvents from gas and liquid phases known as porous magnets and solvatomagnets, respectively [18, 24–29].

Currently, the rapid development of research on photomagnets, molecular magnets revealing change of their magnetic states in the response to external stimuli by electromagnetic radiation (i.e. ultraviolet, visible, and near infrared lights), is also observed. The vast majority of them can be classified as systems showing: organic ligand isomerization or open/close switching with a change of spin state, e.g., stilbenoid complexes, diarylethene type ligands; valence tautomerism, e.g., Co^{II} catecholate; metal-centered thermal spin transition, e.g., Fe^{II}, Mn^{III} spin crossover (SCO) and $[M^{IV}(CN)_8]^{4-}$ (M^{IV} = Mo, W) complexes; metal-to-metal charge transfer (MMCT), e.g., Prussian blue analogues (PBAs); and metal-to-ligand charge transfer (MLCT), e.g., $Na_2[Fe(CN)_5(NO)]\cdot 2H_2O$ and its analogues [30–32]. More importantly, photomagnetic complexes after excitation with light can show the most of nontrivial magnetic behaviors including long-range magnetic ordering [33–36], slow magnetic relaxation [37], or spin transition [38–40], which can be also merged

with other functionalities leading to multifunctional photomagnets [41]. At this point, it is noteworthy to emphasize two multifunctional photomagnets showing spin-crossover-induced SHG, light-reversible spin-crossover, long-range magnetic ordering, and photoswitching of MSHG–$Fe_2[Nb(CN)_8](4\text{-bromopyridine})_8 \cdot 2H_2O$ [42] and a photoswitchable polar magnet that exhibits superionic conduction and SHG–$Cs_{1.1}Fe^{II}_{0.95}[Mo^{I}(CN)_5(NO)] \cdot 4H_2O$ [43].

Another aspect which is important to take into consideration during elucidation of photomagnetic materials is the fact that adding the next factor—excitation light, extends the number of additional experimental parameters that should be carefully considered in research (e.g. light wavelength, intensity, time of irradiation, conditions at which experiment is conducted). Furthermore, the light can also activate diverse mechanisms of photoexcitation which is very exciting but also very challenging to analyze. An excellent example of photomagnetic materials, which can be used in the construction of multifunctional materials, and revealing intricate mechanisms of photomagnetic effect, are Cu^{II}-$[Mo^{IV}(CN)_8]^{4-}$ assemblies [44–50]. Historically, the first attempt to explain the observed photomagnetic phenomenon has been done based on light-induced Metal-to-Metal Charge-Transfer (MMCT) mechanism in Cu^{II}-Mo^{IV} pair [51, 52]. However, because of reported results [53–58], the second mechanism of the Light-Induced Excited Spin-State Trapping (LIESST) effect on $[Mo^{IV}(CN)_8]^{4-}$ anion is also considered. In this work, we would like to guide readers through intriguing research on photomagnetic effect in Cu^{II}-M^{IV} systems.

9.2 Role of the Octacyanidometallate Type in the Photomagnetic Effect

The concept of investigation of the substitution molybdenum for tungsten in photomagnetic copper(II)-octacyanidomolybdate(IV) systems has been considered since the discovery of the phenomenon. Up to the present time, the verification of this idea was unattainable, despite a relatively large number of octacyanidotungstate(IV)-based assemblies [3]. Merely a few works report trials of photoirradiation of Cu(II)-W(IV) samples with light corresponding to absorption bands of these compounds [59]. Unfortunately, none of these studies exhibited any change of magnetic properties upon external stimuli by the visible light. This indicated that this type of assemblies does not present a photomagnetic effect. However, the most recent studies for Mn(II)-W(IV) coordination polymers [53, 54], describing an observation of photomagnetic phenomenon on octacyanidotungstate(IV), again raised expectations for further research.

Presently, there has been a significant step forward in the topic of photomagnetism in Cu(II)-W(IV) assemblies. As a result of self-assembly of two complex salts $[Cu(ida)(H_2O)_2]_n$ (ida^{2-} = iminodiacetate) and $K_4[M(CN)_8] \cdot 2H_2O$ (M = Mo, W), novel layered $K_4\{[Cu^{II}(ida)]_2[M^{IV}(CN)_8]\} \cdot 4H_2O$ (M^{IV} = Mo, W) coordination polymers have been formed (Fig. 9.1) [60]. Both assemblies are isostructural and they are

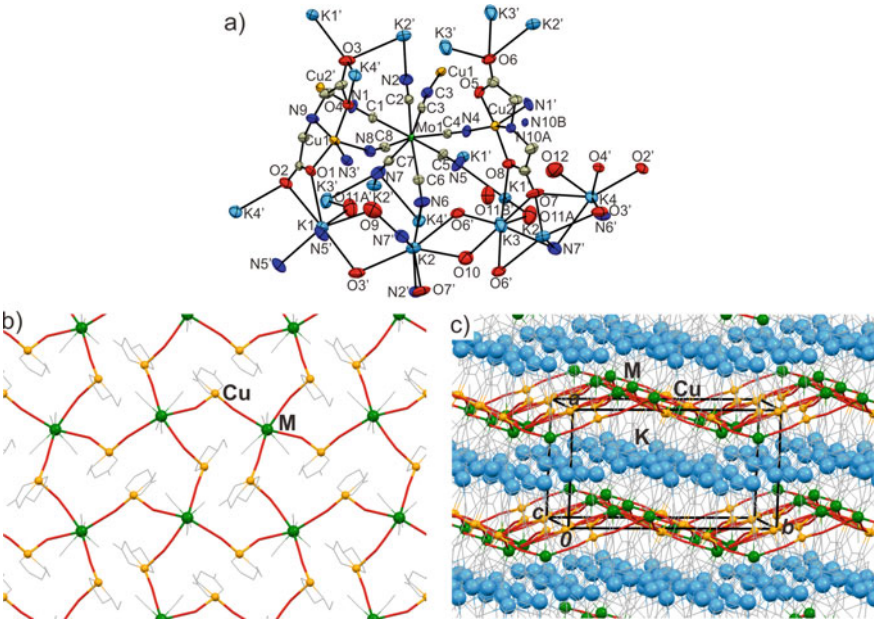

Fig. 9.1 **a** Structural unit of $K_4\{[Cu^{II}(ida)]_2[Mo^{IV}(CN)_8]\}\cdot 4H_2O$. **b** Structure of single layer with cyanido-bridges. **c** Crystal packing. Colors used: K—blue balls; Cu—yellow balls; Mo/W—green balls; bridging CN^-—red sticks; water, ida, and terminal CN^-—gray wireframe. In all figures, hydrogen atoms were omitted for clarity. Reprinted with permission from Inorg. Chem. **59**, 4292 (2020). Copyright 2020 American Chemical Society

rare cases of transition metal complexes with imino acids and polycyanidometallates. Their structures are constructed of a negatively-charged cyanido-bridged square grid with deformed 8-metallic units sandwiching potassium cations and water molecules layers in the analogy to the previously obtained $Cs_2Cu^{II}{}_7[Mo^{IV}(CN)_8]_4\cdot 6H_2O$ system [48]. Additionally, these newly obtained materials characterize complex hydrogen-bond networks and weak Coulomb interactions between potassium cations and lone pairs on oxygen atoms of water molecules and ida^{2-} anions stabilizing their crystal structures. It is also worth highlighting that $K_4\{[Cu^{II}(ida)]_2[M^{IV}(CN)_8]\}\cdot 4H_2O$ coordination polymers adopt two-dimensional topologies which have a greater preference for clearly exhibiting the photomagnetic effect.

Reflectance spectroscopy of $K_4\{[Cu^{II}(ida)]_2[M^{IV}(CN)_8]\}\cdot 4H_2O$ in UV–visible and near-IR regions revealed that structures of both spectra are comparable and complex which can be deconvoluted into ten Gaussian components. All this absorption bands can be assigned to ligand field bands of two symmetry independent $[Cu(ida)(NC)_2]$ units (600–800 nm region), ligand field bands of octacyanidometallate (330–500 nm region), and ligand field and metal-to-ligand charge-transfer bands of $[M(CN)_8]^{4-}$ and to ligand-to-metal charge-transfer bands of $[Cu(ida)(NC)_2]$ units (below 300 nm). Interestingly, all maxima of absorption bands of molybdenum analog are shifted to higher energy. This interpretation of both spectra was applied in the

choice of the excitation wavelengths: 532 and 473 nm laser lines—to observe possible the metal-to-metal charge-transfer photomagnetic effect in the Cu^{II}-M^{IV} pairs, and 407 nm light—to detect prospective Light-Induced Excited Spin-State Trapping in the M^{IV} centers.

Preliminary magnetic studies confirmed that both compounds in their ground state show paramagnetic behavior originating from copper(II) centers with single unpaired electrons ($S_{Cu(II)} = 1/2$, $g_{Cu(II)} = 2.05$) separated by bridging diamagnetic octacyanidometallate anions ($S_{M(IV)} = 0$). At low temperatures, Cu(II) centers interacting antiferromagnetically via the superexchange mechanism giving almost identical magnetic coupling constant zJ' of -0.27 and -0.25 cm^{-1} for Mo and W compounds, respectively. The next photomagnetic experiments for both systems with 407, 473, 532, 658, 705, and 804 nm laser lines have been conducted, however, the response was detected only for excitations with 407 nm. The $K_4\{[Cu^{II}(ida)]_2[Mo^{IV}(CN)_8]\}\cdot 4H_2O$ complex after 24 h of irradiation exhibited 30% increase of product of magnetic susceptibility in the $\chi_M T(T)$ plot and 6% augment of magnetization in the $M(H)$ curve in respect to its initial paramagnetic state (Fig. 9.2). These values are slightly lower than determined ones for other previously reported layered photomagnetic materials. Nonetheless, it is more important to emphasize the first observation of the photomagnetic effect in Cu^{II}-$[W^{IV}(CN)_8]^{4-}$ entities. After 24 h of irradiation with

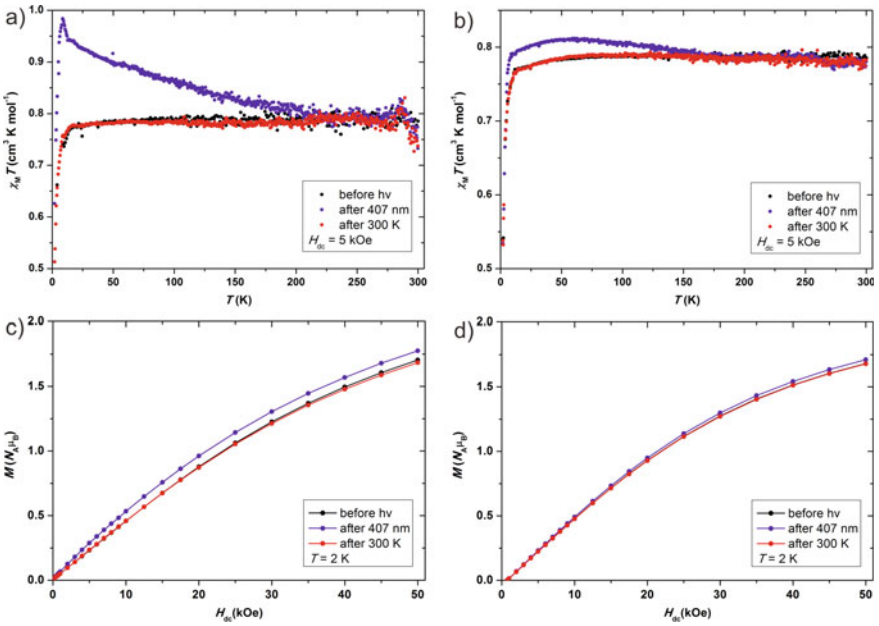

Fig. 9.2 The $\chi_M T(T)$ plots for $K_4\{[Cu^{II}(ida)]_2[M^{IV}(CN)_8]\}\cdot 4H_2O$ (M = Mo—**a**, and W—**b**) before, after excitation with 407 nm light for 24 h, and after thermal relaxation at 300 K; and corresponding $M(H)$ plots determined in the same way for Mo (**c**) and W (**d**) systems. Reprinted with permission from Inorg. Chem. **59**, 4292 (2020). Copyright 2020 American Chemical Society

407 nm light, the growth of $\chi_M T$ and M reached 3 and 2%, respectively. These small but non-negligible values are very important since they motivate further research in the field of photoswitchable materials and they could help in the development of more efficient and stable systems. Additionally, it is also worth highlighting that $\chi_M T(T)$ curves for both compounds differ in shape and relaxation temperature above which compound relax to its initial state before photoirradiation. The $\chi_M T(T)$ plot for octacyanidomolybdate-based system has a clear maximum around 9 K and monotonously diminished up to 230 K while the plot for tungsten analogue has very broad peak up to 160 K without an obvious maximum. The 70 K difference in relaxation temperature demands more studies to confirm if it is common for systems with diverse octacyanidometallates.

Furthermore, the possible mechanism of photomagnetic effect in $K_4\{[Cu^{II}(ida)]_2[M^{IV}(CN)_8]\}\cdot 4H_2O$ (M^{IV} = Mo, W) have been considered based on the most recent knowledge in this research field. Nowadays, two possible mechanisms of photomagnetic phenomenon in Cu(II)-Mo(IV) are advocated. Primarily, this unique phenomenon has been interpreted in the term of light-induced Metal-to-Metal Charge-Transfer (MMCT) mechanism in which spins are reorganized within isolated polynuclear molecules in the course of the following photoreaction: $\{Cu^{II}$ $(S = ½)$-N≡C-Mo^{IV} $(S = 0)$-$[N\equiv C\text{-}Cu^{II}$ $(S = ½)]_n\} \rightarrow \{Cu^{I}$ $(S = 0)$-N≡C-Mo^{V} $(S = ½)$-$[N\equiv C\text{-}Cu^{II}$ $(S = ½)]_n\}$. Consequently, a ferromagnetic coupling within Mo^{V} $(S = ½)$-$[N\equiv C\text{-}Cu^{II}$ $(S = ½)]_n$ units occurred resulting in the formation of local magnetic domains and a maximum in the product of magnetic susceptibility and temperature ($\chi_M T$) *versus* temperature plots. This concept correlated with the most experimental data, however, there was a controversy associated with the unexplained 10% or more increase of magnetic signal at low temperature in high fields after irradiation which ought not to be observed in systems with an invariant number of spins. In response to this inconsistency, a counter-proposals mechanism, explaining photomagnetic effect by means of Light-Induced Excited Spin-State Trapping (LIESST) in the Mo^{IV} centers, has been proposed. In this case the excitation with visible light leads to change of low-spin $Mo^{IV}{}_{LS}$ $(S = 0)$ closed shell singlet centers to high-spin $Mo^{IV}{}_{HS}$ $(S = 1)$ triplet state one, generating $\{Cu^{II}$ $(S = ½)$-N≡C-$Mo^{IV}{}_{HS}$ $(S = 1)$-$[N\equiv C\text{-}Cu^{II}$ $(S = ½)]_n\}$ domains. This idea soon attracted considerable attention and found supporters. Detailed analysis of available data for Cu(II)-Mo(IV) assembly suggested that observed effect can be explained well by LIESST with minor contribution of MMCT mechanism. This conclusion is supported by facts that ligand field bands of $[Mo(CN)_8]^{4-}$ as well as metal-to-ligand charge-transfer bands in Cu^{II}-$[Mo(CN)_8]^{4-}$ pairs can be activated by 407 nm light excitation, and the 6% increase of magnetization in $M(H)$ curve can be achieved only for LIESST mechanism, however, the expected $\chi_M T$ value of 0.9 cm^3 K mol^{-1} at low temperatures will be insufficient to explain observed signal without taking into account minor contribution of MMCT mechanism. Due to lower efficiency of photomagnetic effect in case of Cu^{II}-$[W(CN)_8]^{4-}$ system analysis of mechanism is more challenging and it gave two possible answers that photomagnetic process is related to low efficient LIESST effect on W(IV) or low efficient MMCT mechanism which requires further investigation.

9.3 Influence of Excitation Wavelength on the Mechanism of Photomagnetic Effect and Photoreversibility

An alternative way to tune photomagnetic characteristics of copper(II)-octacyanidomolybdate(IV) compounds are the adjustment of irradiation wavelength. This simple approach allows for the direct enhance of the phenomenon efficiency as well as to generate photoreversibility-phenomenon in which compounds switch back to their ground magnetic state by external stimuli with electromagnetic waves.

The most extensive studies on the influence of different excitation lights on photomagnetic effects have been performed for complex cyanido-bridged molecular ribbon $[Cu^{II}(bapa)]_2[Mo^{IV}(CN)_8]\cdot 7H_2O$, where bapa = bis(3-aminopropyl)amine [46]. This compound is built of two types of complex nodes: trigonal bipyramidal $\{[Cu(bapa)]_3[Mo(CN)_8]_2\}^{2-}$ and rhomboidal $\{[Cu(bapa)]_2[Mo(CN)_8]_2\}^{4-}$ units which are linked through $[Cu(bapa)]^{2+}$ complex ions (Fig. 9.3). Furthermore, hydrogen-bond networks stabilize the structure due to interactions between cyanides organic ligands and water molecules. Moreover, this assembly displays one of the highest complexities among the 1-D chains based on 3d metals with octacyanidometallates and other cyanido bridged complexes.

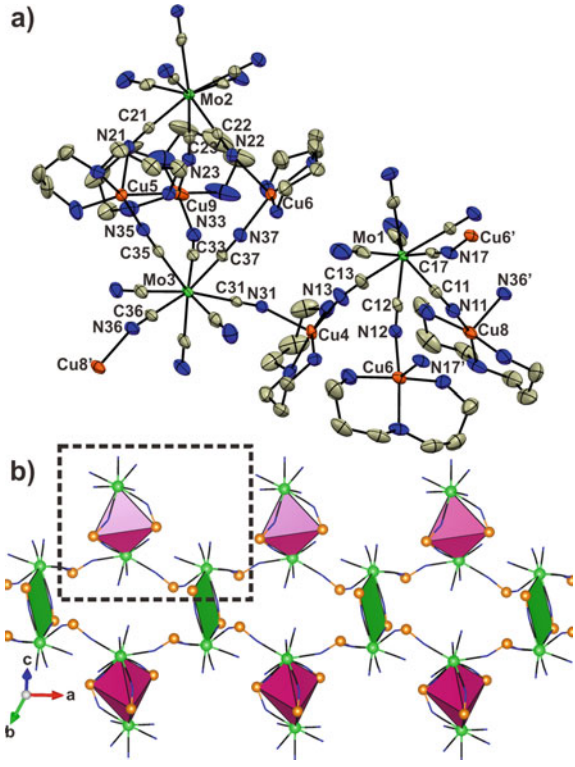

Fig. 9.3 **a** Structural unit of $[Cu^{II}(bapa)]_2[Mo^{IV}(CN)_8]\cdot 7H_2O$. **b** Skeleton of the 1-D ribbon. In both figures, hydrogen atoms and water molecules were omitted for clarity. Reproduced from J. Mater. Chem. C **3**, 8712 (2015) with permission from The Royal Society of Chemistry

Solid state UV–Vis-NIR absorption spectroscopy of $[Cu^{II}(bapa)]_2[Mo^{IV}(CN)_8]\cdot 7H_2O$ revealed several absorption bands assigned to the ligand field bands of $[Cu(bapa)]^{2+}$ complexes with diverse geometries (650–900 nm region), the metal-to-metal charge-transfer band in the Cu^{II}-Mo^{IV} pairs (band around 466 nm), and the ligand field bands of the $[Mo(CN)_8]^{4-}$ in UV region. This assignment agrees with previous observations for other Cu^{II}-$[Mo^{IV}(CN)_8]^{4-}$ systems. The provided interpretation of the spectrum was utilized for the choice of irradiation lights for photomagnetic studies.

From magnetic properties, $[Cu^{II}(bapa)]_2[Mo^{IV}(CN)_8]\cdot 7H_2O$ is ordinary paramagnet, built of copper(II) centers ($S_{Cu(II)} = 1/2$, $g_{Cu(II)} \approx 2.0$) linked by diamagnetic octacyanidomolybdate(IV) anions, revealing very weak antiferromagnetic coupling at low temperature. Nonetheless, this material is a textbook example of the multi-wavelength light-responsive photomagnet. The photomagnetic effect in $[Cu^{II}(bapa)]_2[Mo^{IV}(CN)_8]\cdot 7H_2O$ can be induced by photoexcitation with monochromatic light (405 and 532 nm), and remarkably, with polychromatic white light (Fig. 9.4). This phenomenon is seen as more than 50% and around 43% increase of $\chi_M T$ values after almost one day of illumination with mono- and polychromatic lights, respectively, and it generated several percent increases of saturation magnetization at 1.8 K for all of the light sources (Fig. 9.5). Additionally, it is worth to underline that $\chi_M T(T)$ curves for photoexcited metastable state show similar shapes with maxima around 10 K and monotonous decay up to relaxation temperature around 250 K, above which the sample returns to its initial paramagnetic state.

Complementary photomagnetic research done at 100 K with 405 nm excitation light was also the first attempt for systematic examination of the cause of temperature at which compound is irradiated on the characteristics of photomagnetic phenomenon in the hybrid inorganic–organic compound. This successful experiment revealed no significant difference in results of studies at 10 and 100 K suggesting that the

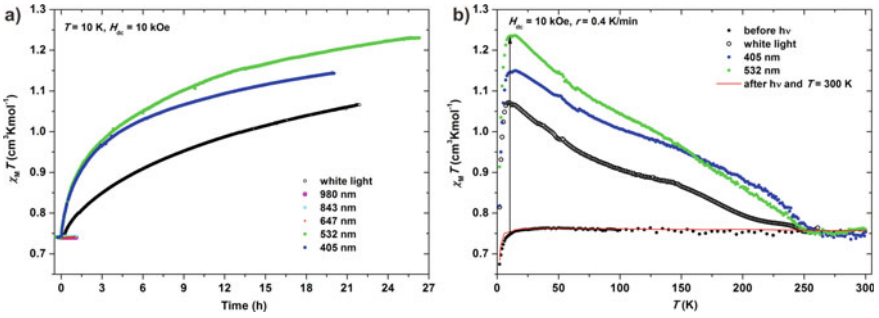

Fig. 9.4 **a** The $\chi_M T$(time) plots of $[Cu^{II}(bapa)]_2[Mo^{IV}(CN)_8]\cdot 7H_2O$ during excitation at 10 K with selected wavelengths and polychromatic white light. **b** The $\chi_M T(T)$ curves before and after excitations with different light sources, and after heating to 300 K. Reproduced from J. Mater. Chem. C **3**, 8712 (2015) with permission from The Royal Society of Chemistry

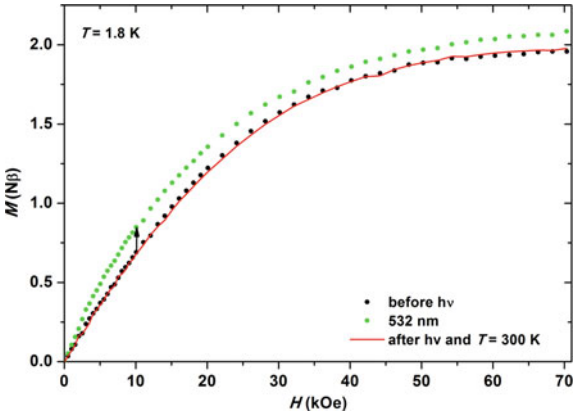

Fig. 9.5 The $M(H)$ plot at 1.8 K for $[Cu^{II}(bapa)]_2[Mo^{IV}(CN)_8]\cdot 7H_2O$ before and after excitation with a 532 nm laser line, and after heating to 300 K. Reproduced from J. Mater. Chem. C **3**, 8712 (2015) with permission from The Royal Society of Chemistry

same magnetic species have been formed and it opens the possibility of commercial use of this material using liquid nitrogen cooling systems (Fig. 9.6). Finally, $[Cu^{II}(bapa)]_2[Mo^{IV}(CN)_8]\cdot 7H_2O$ has been also tested for the photoreversibility effect (Fig. 9.7). In the first stage, a positive photomagnetic effect was induced with the use of green light. After it, using the sequence of light sources (647, 843, and 980 nm) for which no photomagnetic effect was found, the magnetic signal partial reduction was forced. This photoreversible effect has been canceled by repeated illumination with a green light.

The mechanism of photomagnetic and photoreversible processes have been analyzed in the context of two previously mentioned LIESST and MMCT mechanisms. However, the mechanism could not be clearly defined due to insufficient

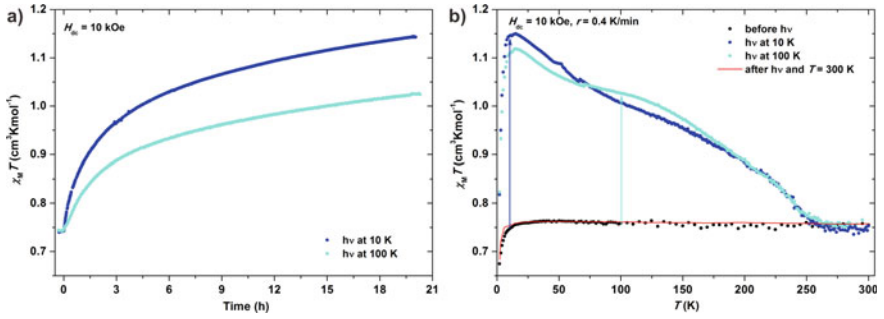

Fig. 9.6 **a** The $\chi_M T$(time) plots of $[Cu^{II}(bapa)]_2[Mo^{IV}(CN)_8]\cdot 7H_2O$ during excitation at 10 and 100 K with 405 nm light. **b** The $\chi_M T(T)$ curves before and after excitations with a 405 nm light done at T = 10 and 100 K, and after heating to 300 K. Reproduced from J. Mater. Chem. C **3**, 8712 (2015) with permission from The Royal Society of Chemistry

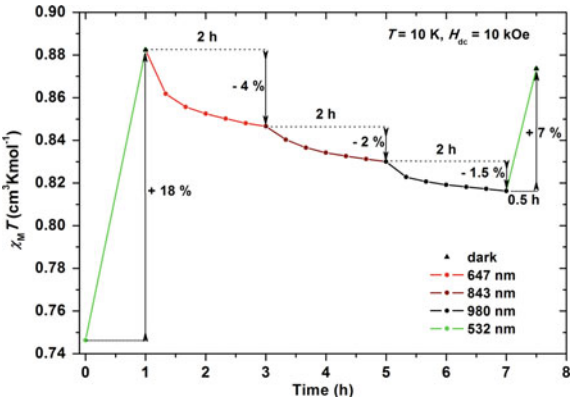

Fig. 9.7 The $\chi_M T$(irradiation time) plots of the photoreversible process at 10 K during subsequent irradiation with 532, 647, 843, and 980 nm laser lines. Reproduced from [46] with permission from The Royal Society of Chemistry

experimental evidence and the high complexity of the system. It was only found out that the mechanism was probably associated mainly with LIESST one with a minor contribution of MMCT process.

Another instance of photomagnetic material reveling photoreversibility-phenomenon is cyanido-bridged layered $[Cu^{II}(cyclam)]_2[Mo^{IV}(CN)_8]\cdot 10H_2O$ coordination polymer, where cyclam = 1,4,8,11-tetraazacyclodecane [34]. The crystal structure consists of neutral square grids with deformed 8-metallic units separated by water molecules stabilized by hydrogen-bond interactions with cyclam ligands and terminal cyanides (Fig. 9.8).

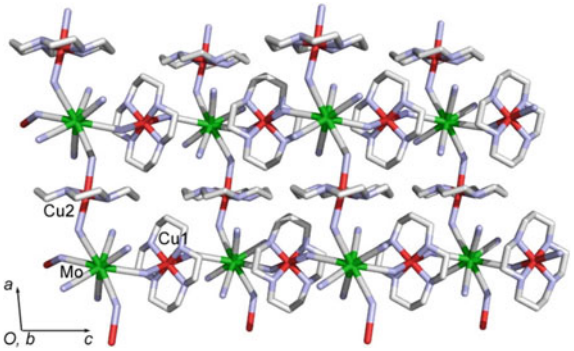

Fig. 9.8 Structure of $[Cu^{II}(cyclam)]_2[Mo^{IV}(CN)_8]\cdot 10H_2O$ single layer with cyanido-bridges. Water molecules are omitted for clarity. Reproduced from Chem. Lett. **38**, 338 (2009) with permission from The Chemical Society of Japan (CSJ)

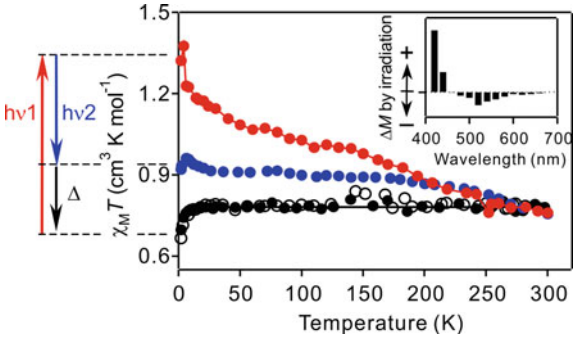

Fig. 9.9 The $\chi_M T(T)$ curves before (white circles), after 410 nm irradiation for 60 min (red circles), after 658 nm irradiation for 300 min (blue circles), and after thermal treatment at 300 K (black circles). Solid black line is to guide the eye. Inset: Wavelength of the laser light *vs.* the change in magnetization. Reproduced from Chem. Lett. **38**, 338 (2009) with permission from The Chemical Society of Japan (CSJ)

This compound before photoirradiation is a paramagnetic system with isolated copper(II) centers ($S_{Cu(II)} = 1/2$, $g_{Cu(II)} \approx 2.0$) showing weak antiferromagnetic interactions below 30 K which is similar to other Cu^{II}-$[Mo^{IV}(CN)_8]^{4-}$ systems. Successive irradiation of the sample with 410 nm blue light at 3 K leads to the monotone increase of magnetization and consecutively to appearance of the broad peak in the $\chi_M T(T)$ curve with maxima around 10 K which continuously decrease up to relaxation temperature above 250 K. Further heating induces complete recovery of sample to their primary paramagnetic state. But even more interestingly, if the sample in its photoinduced metastable state is illuminated with 658 nm red light, the $\chi_M T$ value diminishes partially, however no lower than the level before the photomagnetic experiment (Fig. 9.9). This photoreversible process was also observed in infrared spectroscopy as a modulation structure and intensities of the CN^- stretching frequency bands upon irradiation with different lights and heating up. Photoirradiation of $[Cu^{II}(cyclam)]_2[Mo^{IV}(CN)_8]\cdot 10H_2O$ with 410 nm blue light at 3 K led to a decrease in the intensity of all IR bands in $\nu(C{\equiv}N)$ region, then the application of 658 nm red light increased bands intensities, and finally, the sample reset to its initial state after 3–300–3 K heating and cooling cycle.

Finally, the results of both magnetic and spectroscopic studies were analyzed in the term of light-induced Metal-to-Metal Charge-Transfer (MMCT) mechanism of photomagnetic effect in this compound (Fig. 9.10). The increase of magnetic signal and decrease of the CN^- stretching bands intensities during irradiation with blue light have been interpreted as a consequence of the photoinduced electron transfer from Mo^{IV} to Cu^{II} in the course of the following photoreaction: $[Cu^{II}(cyclam)]_2[Mo^{IV}(CN)_8]\cdot 10H_2O \rightarrow [Cu^{II}(cyclam)]_{2x}[Cu^{I}(cyclam)]_x[Mo^{IV}(CN)_8]_{1-x}[Mo^{V}(CN)_8]_x\cdot 10H_2O$, where $S_{Cu(II)} = S_{Mo(V)} = ½$ and $S_{Cu(I)} = S_{Mo(IV)} = 0$, while revers effects originate in photoinduced back electron transfer by illumination with red light or by thermal treatment.

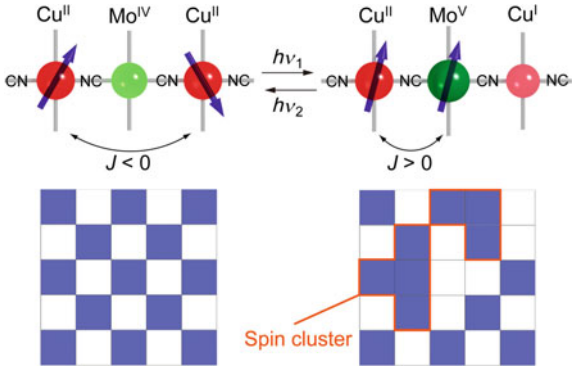

Fig. 9.10 Probable scheme of the photoreversible effect. The diagram shows 2-D Cu-Mo grid layer. Blue and white squares indicate S = 1/2 and S = 0, respectively. Reproduced from Chem. Lett. **38**, 338 (2009) with permission from The Chemical Society of Japan (CSJ)

It is also worth mentioning another experiment for $[Cu^{II}(cyclam)]_2[Mo^{IV}(CN)_8]\cdot 10H_2O$ which has been focused on detection of the 410-nm light photoswitching effect at near-room temperature using infrared spectroscopy [61]. As a result, the change in the intensity of bands in the $\nu(C{\equiv}N)$ region has been observed (Fig. 9.11). A thorough analysis of the data has shown that the photogenerated metastable phase thermally relaxed to the initial state with a half-life time of 27, 69, and 170 s at 293, 283, and 273 K in series which is shorter than a single magnetic measurement period. Near-room temperature photoswitching

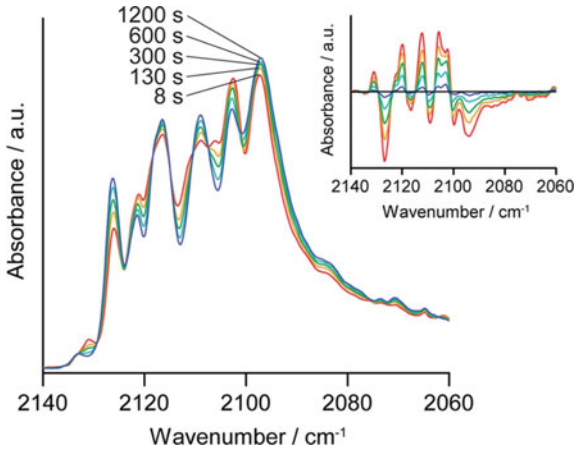

Fig. 9.11 Time dependence of the IR spectra of $[Cu^{II}(cyclam)]_2[Mo^{IV}(CN)_8]\cdot 10H_2O$ at 273 K after excitation. Inset: differential IR spectra before and after light irradiation. Reproduced with permission from AIP Advances 3, 042,133 (2013). Copyright 2013 American Chemical Society

is an essential matter in the field of optical functional materials. This model assembly is useful for the demonstration of high-temperature photoswitching material.

So far presented works showed photoswitching between initial paramagnetic state and metastable photoexcited paramagnetic state. At this point, it is necessary to distinguish another three-dimensional cyanido-bridged coordination polymer $Cu^{II}_2[Mo^{IV}(CN)_8]\cdot 8H_2O$ demonstrating a unique photomagnetic effect [47]. The crystal structure of this material consists of Mo-crosslinked square grids with distorted 4-metallic units and channels field with crystallization and coordination water molecules.

In their ground state $Cu^{II}_2[Mo^{IV}(CN)_8]\cdot 8H_2O$ is paramagnet with weak antiferromagnetic interactions at low-temperature region showing the metal-to-metal charge-transfer band between Mo^{IV}-CN-Cu^{II} and Mo^{V}-CN-Cu^{I} around 480 nm in UV-vis spectrum. Irradiation of the sample with 473 nm blue light at 3 K for 165 min caused the growth of magnetization and the manifestation of a spontaneous magnetization with a Curie temperature (T_C) of 25 K (Fig. 9.12) and magnetic hysteresis with the coercive field of 34 Oe which disappear completely after thermal treatment above 250 K and cooling to 3 K. Moreover, further photomagnetic studies for $Cu^{II}_2[Mo^{IV}(CN)_8]\cdot 8H_2O$ exhibit that the phenomenon can be induced by using laser light below 520 nm (Fig. 9.13), conversely, the light with lower energy is responsible for photoreversible effect. It is worth emphasizing that successive application of 658, 785, and 840 nm lights for photoreversibility studies resulted in complete recovery of initial paramagnetic state without heating above relaxation temperature (Fig. 9.12). These essential observations have also been confirmed in spectroscopic measurements. Infrared spectroscopy for $Cu^{II}_2[Mo^{IV}(CN)_8]\cdot 8H_2O$ revealed that the band at 2170 cm^{-1}, corresponding to Mo^{IV}-CN-Cu^{II}, diminish upon excitation with 473 nm and entirely restore after heating above 250 K. In case of UV-vis absorption

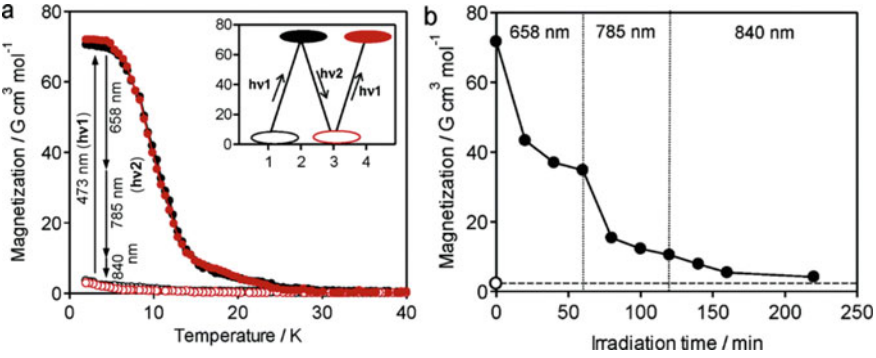

Fig. 9.12 **a** The $M(T)$ plots before (black open circle), after irradiation with 473 nm light (black closed circle), after subsequent irradiation with 658, 785 and 840 nm lights (red open circle) and the second irradiation with 473 nm light (red closed circle). **b** The M(irradiation time) plots of the photoreversible process at 3 K during subsequent irradiation with 473, 658, 785 and 840 nm laser lines. Reprinted with permission from J. Am. Chem. Soc. **128**, 270 (2006). Copyright 2006 American Chemical Society

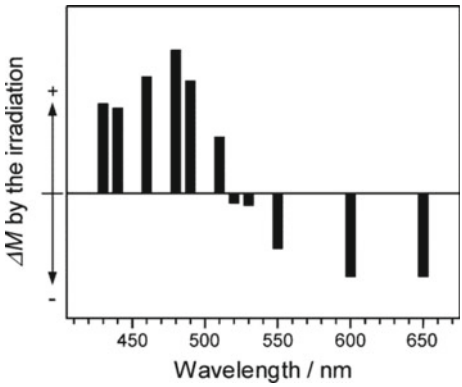

Fig. 9.13 Wavelength of the laser light *vs.* the change in magnetization. Reprinted with permission from J. Am. Chem. Soc. **128**, 270 (2006). Copyright 2006 American Chemical Society

spectroscopy, the response towards 473 nm laser light is also noted. Before irradiation, the spectrum of the compound comprises of the metal-to-ligand charge-transfer bands of $[M(CN)_8]^{4-}$ (250 nm), the ligand field bands of octacyanidometallate (370 and 400 nm), the metal-to-metal charge-transfer band (483 nm) and the ligand field bands of Cu(II) (637, 719 and 855 nm). The irradiation caused the reduction of band intensities and a new broad band to appear in the 600–900 nm region, the opposite characteristics are observed after irradiation with 658, 785 and 840 nm lights sequence or warming above 250 K. This indicates that the new band around 710 nm is the reverse metal-to-metal charge-transfer band from Mo^{V}-CN-Cu^{I} and Mo^{IV}-CN-Cu^{II} species.

All of the evidence indicates that the observed photomagnetic effect is a result of blue light-induced MMCT between ground paramagnetic state $\{Cu^{II}Mo^{IV}Cu^{II}\}_n$ and metastable state $\{Cu^{II}Mo^{V}Cu^{I}\}_n$, showing long-range magnetic ordering due to the photoinduced formation of the extended network of ferromagnetically coupled Mo^{V}-CN-Cu^{II} linkages (Fig. 9.14). This effect can be reversed by heating above the temperature at which the metastable state spontaneously relaxes or by utilizing light corresponding to the photogenerated reverse-MMCT band.

9.3.1 Influence of Photoexcitation Temperature

As already indicated, the parameters of photomagnetic effects can be amplified or weakened at the synthesis stage and by the precise selection of the excitation light wavelengths. Moreover, preliminary investigations for $[Cu^{II}(bapa)]_2[Mo^{IV}(CN)_8]\cdot 7H_2O$ set a new direction for research, which is to broaden knowledge about the influence of temperature at which sample is photoexcited [46]. This work showed that there is no significant difference in the results of photomagnetic studies after excitation at 10 and 100 K (Fig. 9.6).

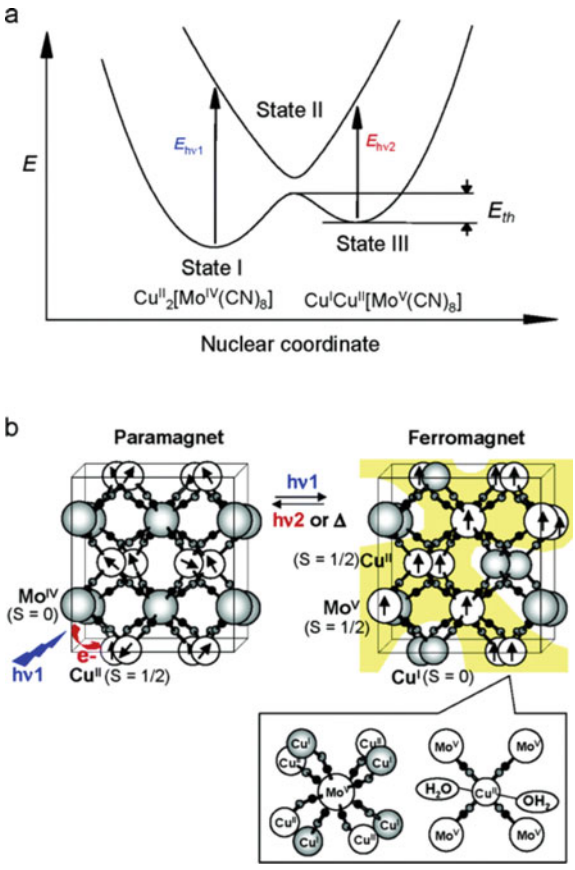

Fig. 9.14 **a** Possible energy diagrams of a class II mixed-valence compound. **b** Probable scheme of the photoreversible effect. The yellow areas show a possible route for the ferromagnetic spin alignment. Reprinted with permission from J. Am. Chem. Soc. **128**, 270 (2006). Copyright 2006 American Chemical Society

Advanced research in this topic has been conducted for a model trinuclear V-shape molecule $[Cu^{II}(enpnen)]_2[Mo^{IV}(CN)_8]\cdot 6.75H_2O$, enpnen = *N,N'*-bis(2-aminoethyl)-1,3-propanediamine (Fig. 9.15) [44]. This system has shown that photomagnetic effect in Cu^{II}-$[Mo^{IV}(CN)_8]^{4-}$ compounds should be analyzed as a combination of both competing MMCT and LIESST effects (Fig. 9.16). Furthermore, this research also unveiled that the ratio between them is correlated with the temperature at which photoexcitation is conducted (Fig. 9.17). At low temperatures, the major part of the magnetic signal is associated to MMCT mechanism with a minor few percent contribution of LIESST. The increase of the temperature leads to diminish and to complete disappearance of MMCT contribution at 100 and 150 K, respectively, without significant change of the fraction of LIESST component. Excitation at 200 K generates only a small contribution of LIESST part.

Detailed analysis of extensive magnetic data for $[Cu^{II}(enpnen)]_2[Mo^{IV}(CN)_8]\cdot 6.75H_2O$ using three models: model "0" for the initial unperturbed ground state $\{Cu^{II}$ (S = ½)-N≡C-$Mo^{IV}{}_{LS}$ (S = 0)-[N≡C-Cu^{II} (S = ½)]$_n$}, model "1" for the MMCT metastable excited state $\{Cu^{I}$ (S =

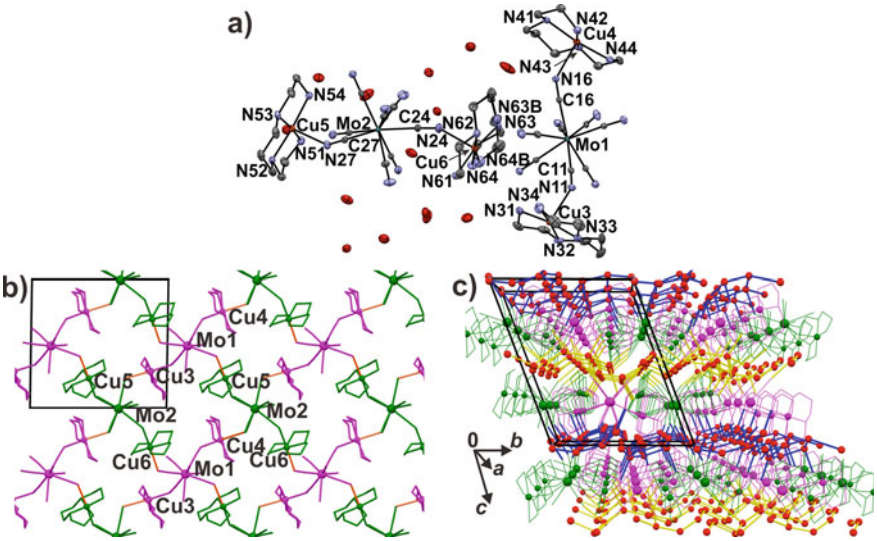

Fig. 9.15 **a** Structural unit of $[Cu^{II}(enpnen)]_2[Mo^{IV}(CN)_8]\cdot 6.75H_2O$. **b** Supramolecular interactions within layers. **c** Crystal packing. Adapted with permission from Inorg. Chem. **57**, 8137 (2018). Copyright 2018 American Chemical Society

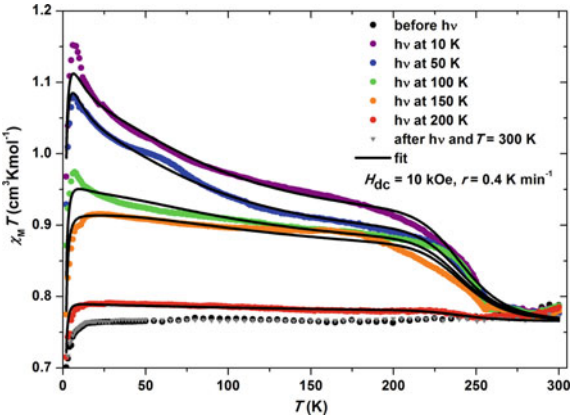

Fig. 9.16 The $\chi_M T(T)$ plots for $[Cu(enpnen)]_2[Mo(CN)_8]\cdot 6.75H_2O$ before and after excitation with 405 nm laser line performed at diverse temperatures, and after heating to 300 K. Solid lines are fits of a model representing the three assumed possible states after irradiation. Adapted with permission from Inorg. Chem. 57, 8137 (2018). Copyright 2018 American Chemical Society

0)-N≡C-Mo^V (S = ½)-[N≡C-Cu^{II} (S = ½)]$_n$}, and model "2" for the LIESST metastable excited state {Cu^{II} (S = ½)-N≡C-$Mo^{IV}{}_{HS}$ (S = 1)-[N≡C-Cu^{II} (S = ½)]$_n$} has been performed (Fig. 9.17). Models "1" and "2" were described by following Hamiltonians: $\hat{H}_1 = -J_1\hat{S}_{Mo}\cdot\hat{S}_{Cu} + g\mu_B\left(\hat{S}_{Cu}+\hat{S}_{Mo}\right)\cdot\vec{H}$ and

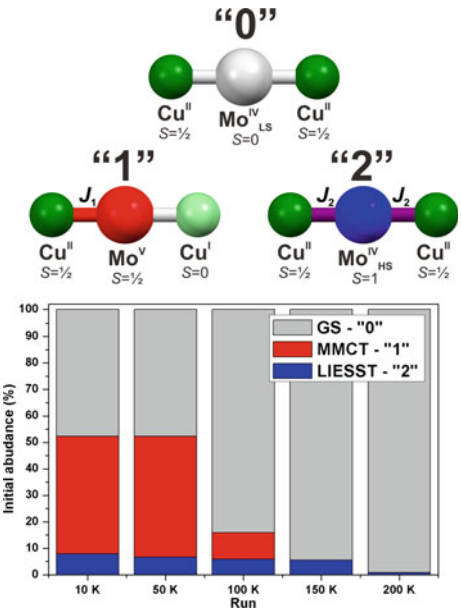

Fig. 9.17 Schematic of the ground state—model "0", the MMCT excited state—model "1" and the LIESST state—model "2", and fractions of the model "0" (GS), model "1" (MMCT) and model "2" (LIESST) states for the irradiation of $[Cu^{II}(enpnen)]_2[Mo^{IV}(CN)_8]\cdot 6.75H_2O$ at different temperatures. Adapted with permission from Inorg. Chem. **57**, 8137 (2018). Copyright 2018 American Chemical Society

$\hat{H}_2 = -J_2\hat{S}_{Mo}\cdot\left(\hat{S}_{Cu1}+\hat{S}_{Cu2}\right)+g\mu_B\left(\hat{S}_{Cu1}+\hat{S}_{Cu2}+\hat{S}_{Mo}\right)\cdot\vec{H}$, respectively, where ${J_1}^{\mathrm{MMCT}}$ and ${J_2}^{\mathrm{LIESST}}$ denote superexchange coupling constants between the Mo^V ($S = ½$) and residual Cu^{II} ($S = ½$) centers, and the $Mo^{IV}{}_{HS}$ ($S = 1$) and Cu^{II} ($S = ½$) centers, respectively, and a single average Landé factor g. As a result of fits, $\chi_M T(T)$ and $M(H)$ curves after excitations at different temperature have been reproduced with the general good compatibility between the observed and calculated values, and ${J_1}^{\mathrm{MMCT}}$ and ${J_2}^{\mathrm{LIESST}}$ values of 11 cm^{-1} and 109 cm^{-1}, respectively, and $g = 2.13(2)$ were determined. Furthermore, these fits revealed that the lifetime of photoinduced MMCT metastable state at low temperature and the relaxation energy barrier ($\Delta_1 \approx 100$ K) are sufficient to treat it as a stable state for long period, however, at higher temperatures (around 100 K) it spontaneously returns to the ground state within the experiment time span. The identical relaxation effect but at the higher temperature (around 200 K) is remarked for LIESST metastable state due to higher energy barrier ($\Delta_2 \approx 4400$ K) and larger value of the high-temperature limit of the lifetime. The estimated threshold temperature of the decay of the metastable state process is 243(7) K which is in agreement with the experimentally evaluated relaxation temperature of 255 K. Finally, these calculations also provided reliable information about the fractions of each model achieved in each experimental conditions. Concluding, this work broaden knowledge about the potential mechanism of photomagnetic effect in Cu^{II}-$[Mo^{IV}(CN)_8]^{4-}$ systems and it stressed the impact of experimental conditions (temperature) on the result of photomagnetic studies which was barely investigated.

This chapter gathers the most vivid examples of experimental factors impacting on photomagnetic effect in Cu^{II}-$[M^{IV}(CN)_8]^{4-}$ complexes. Here, we show that the exchange of octacyanidomolybdate with octacyanidotungstate can modify the intensity of photomagnetic signals and relaxation temperatures. Furthermore, the influence of irradiation wavelength and photoexcitation temperature has been also studied, resulting in the observation that different photomagnetic responses and phenomena mechanisms can be controlled at the level of experiment design. These findings will allow researchers to consider novel factors allowing for more sophisticated control of photomagnetic characteristics.

References

1. L. Ouahab (ed.), *Multifunctional Molecular Materials* (Pan Stanford, Singapore, 2013).
2. S.M. Mukhopadhyay (ed.), *Nanoscale Multifunctional Materials: Science and Applications* (Wiley, New Jersey, 2012)
3. B. Nowicka, T. Korzeniak, O. Stefańczyk, D. Pinkowicz, S. Chorąży, R. Podgajny, B. Sieklucka, Coord. Chem. Rev. **256**, 1946 (2012)
4. S. Ohkoshi, in *Progress in Photon Science: Basics and Applications (Springer Series in Chemical Physics Book 115)*. ed. by K. Yamanouchi (Springer International Publishing AG, Cham, 2017), p. 263
5. K. Nakabayshi, S. Ohkoshi, S. Chorazy, in *Progress in Photon Science: Recent Advances (Springer Series in Chemical Physics Book 119)*. ed. by K. Yamanouchi, S. Tunik, V. Makarov (Springer International Publishing AG, Cham, 2019), p. 453
6. M. Reczyński, K. Nakabayashi, S. Ohkoshi, Tuning the Optical Properties of Magnetic Materials. Eur. J. Inorg. Chem. (2020). https://doi.org/10.1002/ejic.202000428
7. H. Tokoro, S. Ohkoshi, Dalton Trans. **40**, 6825 (2011)
8. C. Train, M. Gruselle, M. Verdaguer, Chem. Soc. Rev. **40**, 3297 (2011)
9. S. Chorazy, R. Podgajny, W. Nitek, T. Fic, E. Görlich, M. Rams, B. Sieklucka, Chem. Commun. **49**, 6731 (2013)
10. K. Inoue, K. Kikuchi, M. Ohba, H. Okawa, Angew. Chem. Int. Ed. **42**, 4810 (2003)
11. C. Train, R. Gheorghe, V. Krstic, L.-M. Chamoreau, N.S. Ovanesyan, G.L.J.A. Rikken, M. Gruselle, M. Verdaguer, Nat. Mater. **7**, 729 (2008)
12. T. Nuida, T. Matsuda, H. Tokoro, S. Sakurai, K. Hashimoto, S. Ohkoshi, J. Am. Chem. Soc. **127**, 11604 (2005)
13. D. Pinkowicz, R. Podgajny, W. Nitek, M. Rams, A.M. Majcher, T. Nuida, S. Ohkoshi, B. Sieklucka, Chem. Mater. **23**, 21 (2011)
14. Y. Tsunobuchi, W. Kosaka, T. Nuida, S. Ohkoshi, CrystEngComm **11**, 2051 (2009)
15. M. Komine, K. Imoto, Y. Miyamoto, K. Nakabayashi, S. Ohkoshi, Eur. J. Inorg. Chem. **1367** (2018).
16. C. Train, T. Nuida, R. Gheorghe, M. Gruselle, S. Ohkoshi, J. Am. Chem. Soc. **131**, 16838 (2009)
17. J. Wang, J. Zakrzewski, M. Heczko, M. Zychowicz, K. Nakagawa, K. Nakabayashi, B. Sieklucka, S. Chorazy, S. Ohkoshi, J. Am. Chem. Soc. **142**, 3970 (2020)
18. Y. Xin, J. Wang, M. Zychowicz, J. Zakrzewski, K. Nakabayashi, B. Sieklucka, S. Chorazy, S. Ohkoshi, J. Am. Chem. Soc. **141**, 18211 (2019)
19. S. Chorazy, J.J. Zakrzewski, M. Reczynski, K. Nakabayashi, S. Ohkoshi, B. Sieklucka J. Mater. Chem. C **7**, 4164 (2019)
20. E. Chelebaeva, J. Larionova, Y. Guari, R.A.S. Ferreira, L.D. Carlos, F.A. Almeida Paz, A. Trifonov, C. Guerin, Inorg. Chem. **48**, 5983 (2009)

21. E. Pardo, C. Train, H. Liu, L.M. Chamoreau, B. Dhkil, K. Boubekeur, F. Lloret, K. Nakatani, H. Tokoro, S. Ohkoshi, M. Verdaguer, Angew. Chem. Int. Ed. **51**, 8356 (2012)
22. S. Ohkoshi, H. Tokoro, T. Matsuda, H. Takahashi, H. Irie, K. Hashimoto, Angew. Chem. Int. Ed. **46**, 3238 (2007)
23. S. Ohkoshi, K. Nakagawa, K. Tomono, K. Imoto Y. Tsunobuchi, H. Tokoro, J. Am. Chem. Soc. **132**, 6620 (2010)
24. S. Ohkoshi, A. Namai, H. Tokoro, Coord. Chem. Rev. **380**, 572 (2019)
25. O. Stefanczyk, S. Ohkoshi, Chem. Eur. J. **25**, 15963 (2019)
26. K.K. Orisaku, O. Stefanczyk, S. Ohishi, N. Ozaki, Y. Miyamoto, K. Imoto, S. Ohkoshi, Chem. Eur. J. **25**, 11066 (2019)
27. M. Reczynski, B. Nowicka, C. Nather, M. Koziel, K. Nakabayashi, S. Ohkoshi, B. Sieklucka, Inorg. Chem. **57**, 13415 (2018)
28. M. Reczyński, S. Chorazy, B. Nowicka, B. Sieklucka, S. Ohkoshi, Inorg. Chem. **56**, 179 (2017)
29. S. Ohkoshi, K. Arai, Y. Sato, K. Hashimoto, Nat. Mater. **3**, 857 (2004)
30. B. Sieklucka, D. Pinkowicz (eds.), *Molecular Magnetic Materials: Concepts and Applications* (Wiley-VCH, Wienheim, 2017)
31. M.A. Halcrow, *Spin-Crossover Materials: Properties and Applications* (Wiley, Chichester, 2013).
32. P. Gütlich, Y. Garcia, T. Woike, Coord. Chem. Rev. **219–221**, 839 (2001)
33. S. Ohkoshi, K. Imoto, Y. Tsunobuchi, S. Takano, H. Tokoro, Nat. Chem. **3**, 564 (2011)
34. H. Tokoro, K. Nakagawa, K. Nakabayashi, T. Kashiwagi, K. Hashimoto, S. Ohkoshi, Chem. Lett. **38**, 338 (2009)
35. S. Ohkoshi, Y. Hamada, T. Matsuda, Y. Tsunobuchi, H. Tokoro. Chem. Mater. **20**, 3048 (2008)
36. S. Ohkoshi, S. Ikeda, T. Hozumi, T. Kashiwagi, K. Hashimoto, J. Am. Chem. Soc. **128**, 5320 (2006)
37. C. Mathonière, H.-J. Lin, D. Siretanu, R. Clérac, J.M. Smith J. Am. Chem. Soc. **135**, 19083 (2013)
38. C. Mathoniere, Eur. J. Inorg. Chem. **248** (2018)
39. E.S. Koumousi, I.-R. Jeon, Q. Gao, P. Dechambenoit, D.N. Woodruff, P. Merzeau, L. Buisson, X. Jia, D. Li, F. Volatron, C. Mathonière, R. Clérac, J. Am. Chem. Soc. **136**, 15461 (2014)
40. O.N. Risset, P.A. Quintero, T.V. Brinzari, M.J. Andrus, M.W. Lufaso, M.W. Meisel, D.R. Talham, J. Am. Chem. Soc. **136**, 15660 (2014)
41. S. Ohkoshi, H. Tokoro, Accounts Chem. Res. **45**, 1749 (2012)
42. S. Ohkoshi, S. Takano, K. Imoto, M. Yoshikiyo, A. Namai, H. Tokoro, Nat. Photonics **8**, 65 (2014)
43. S. Ohkoshi, K. Nakagawa, K. Imoto, H. Tokoro, Y. Shibata, K. Okamoto, Y. Miyamoto, M. Komine, M. Yoshikiyo, A. Namai. Nat. Chem. **12**, 338 (2020)
44. O. Stefańczyk, R. Pełka, A.M. Majcher, C. Mathonière, B. Sieklucka, Inorg. Chem. **57**, 8137 (2018)
45. Y. Umeta, S. Chorazy, K. Nakabayashi, S. Ohkoshi, Eur. J. Inorg. Chem. **1980** (2016)
46. O. Stefańczyk, A.M. Majcher, M. Rams, W. Nitek, C. Mathonière, B. Sieklucka, J. Mater. Chem. C **3**, 8712 (2015)
47. S. Ohkoshi, H. Tokoro, T. Hozumi, Y. Zhang, K. Hashimoto, C. Mathonière, I. Bord, G. Rombaut, M. Verelst, C. Cartier dit Moulin, F. Villain, J. Am. Chem. Soc. **128**, 270 (2006)
48. T. Hozumi, K. Hashimoto, S. Ohkoshi, J. Am. Chem. Soc. **127**, 3864 (2005)
49. X.-D. Ma, T. Yokoyama, T. Hozumi, K. Hashimoto, S. Ohkoshi, Phys. Rev. B **72**, 094107(6) (2005)
50. J.-M. Herrera, V. Marvaud, M. Verdaguer, J. Marrot, M. Kalisz, C. Mathonière, Angew. Chem. Int. Ed. **43**, 5468 (2004)
51. G. Rombaut, M. Verelst, S. Golhen, L. Ouahab, C. Mathonière, O. Kahn, Inorg. Chem. **40**, 1151 (2001)
52. S. Ohkoshi, N. Machida, Y. Abe, Z.J. Zhong, K. Hashimoto, Chem. Lett. **4**, 312 (2001)
53. X. Qi, S. Pillet, C. de Graaf, M. Magott, E.-E. Bendeif, P. Guionneau, M. Rouzières, V. Marvaud, O. Stefańczyk, D. Pinkowicz, C. Mathonière, Angew. Chem. Int. Ed. **59**, 3117 (2020)

54. M. Magott, M. Reczyński, B. Gaweł, B. Sieklucka, D. Pinkowicz, J. Am. Chem. Soc. **140**, 15876 (2018)
55. M. Magott, O. Stefanczyk, B. Sieklucka, D. Pinkowicz, Angew. Chem. Int. Ed. **43**, 13283 (2017)
56. N. Bridonneau, J. Long, J.-L. Cantin, J. von Bardeleben, S. Pillet, E.-E. Bendeif, D. Aravena, E. Ruiz, V. Marvaud, Chem. Commun. **51**, 8229 (2015)
57. S. Brossard, F. Volatron, L. Lisnard, M.-A. Arrio, L. Catala, C. Mathonière, T. Mallah, C. Cartier dit Moulin, A. Rogalev, F. Wilhelm, A. Smekhova, P. Sainctavit, J. Am. Chem. Soc. **134**, 222 (2012)
58. M.-A. Arrio, J. Long, C. Cartier dit Moulin, A. Bachschmidt, V. Marvaud, A. Rogalev, C. Mathonière, F. Wilhelm, P. Sainctavit, J. Phys. Chem. C **114**, 593 (2010)
59. O. Stefańczyk, M. Rams, A.M. Majcher, C. Mathonière, B. Sieklucka, Inorg. Chem. **53**, 3874 (2014)
60. O. Stefanczyk, S. Ohkoshi, Inorg. Chem. **59**, 4292 (2020)
61. Y. Umeta, H. Tokoro, N. Ozaki, S. Ohkoshi. AIP Adv. **3**, 042133 (2013)